UNIVERSITY OF CALIFORNIA, SAN DIEGO

Solution Grown Antimony Doped Zinc Oxide Films

A Thesis submitted in partial satisfaction of the requirements for the degree

Master of Science

in

Chemical Engineering

by

Conor T. Riley

Committee in charge:

Professor Deli Wang, Chair
Professor Richard K. Herz
Professor Jan Talbot
Professor Joanna McKittrick

2012

The Thesis of Conor T. Riley is approved and it is acceptable in quality and form for publication on microfilm and electronically:

_____

_____

_____

_____

Chair

University of California, San Diego

2012

In dedication to the memory of my father, Kevin Joseph Riley

TABLE OF CONTENTS

LIST OF FIGURES

LIST OF TABLES

ACKNOWLEDEMENTS

Foremost, I would like to thank my supervisor Prof. Deli Wang for his priceless guidance throughout the duration of this research. Without his knowledge and support this research would not have been a possibility. I would also like to thank Prof. Richard K. Herz, Prof. Jan Talbot and Prof. Joanna McKittrick for serving on my committee. I also appreciate the time our collaborators Penghui Guo and Shaohua Shen at Xi'an Jiaotong University have taken to provide XPS measurements of the samples. In addition I would like to thank Prof. Paul Yu for allowing us to use his hall measurement equipment. Last but not least I would like to thank my colleagues Ke Sun, Namseok Park, Siarhei Vishniakou, Zhelin Sun, Brian Lewis, Muchuan Yang, Alireza Kargar, Sonia Noh, Yi Jing for the many discussions on zinc oxide growth and device fabrication. In particular I would like to acknowledge Ke Sun and Namseok Park for the Hall measurements and Zhelin Sun for the AFM measurements.

VITA

Education

M.S. Chemical Engineering, University of California, San Diego
Expected graduation date, May, 2012
Department of Chemical engineering
GPA 3.55/4.0

B.S. Chemical Physics, University of California, San Diego
December, 2007
Chemistry departmental honors
Provost's Honors List 2005-2006
GPA 3.61/4.0

Professional Experience

Researcher, Graduate, University of California, San Diego (D. Wang Lab) (1/11-present)
Research and development of solution grown doped zinc oxide nanowires and thin films. Characterization of electrical properties and development of devices exploiting p and n-type behavior of doped materials.

Research Associate, Wildcat Discovery Technologies, 5/2008-8/2010
Research, synthesis and characterization of materials for fuel cells, lithium ion batteries and hydrogen storage. Key member in implementation of high throughput discovery systems.

Materials science intern, Nitto Denko Technologies, 12/07-5/2008
Preparation and analysis of thin-film semiconducting materials to develop solar devices.

Researcher, undergraduate, University of California, San Diego (Kubiak Group) 8/2007-12/2007
Synthesis and analysis of various (diene)$Fe(CO)_3$ compounds to investigate IR peak coalescence at elevated temperatures.

Researcher, undergraduate, University of California, San Diego (McCammon group) 9/2006-12/2007
Implementation of molecular dynamics simulations using gromos96 software package. Preparation and analysis of results using C-shell and python.

Publications
1. Baron R., **Riley C**., Chenprakhon P., Thotsaporn K, Winter R.T., Alfieri A., Forneris F., van Berkel W.J.H., Chaiyen P., Fraaije M.W., Mattevi A., McCammon J.A. Multiple pathways guide oxygen diffusion into flavoenzyme active sites. Proc. Natl. Acad. Sci. USA, 2009; 106: 10603-10608.

Patents
1. Kaye, S. , **Riley, C**. Method of preparing boron-nitrogen compounds. US patent application 61/242932, 2009.

2. Li, B., Kaye, S., **Riley, C.,** Greenberg, D., Lithium ion battery materials with improved properties. US patent application No. 61/426,733.

Scientific Presentations
1. The Diffusion of Small Molecules into Flavoproteins as Revealed by Enhanced-Diffusion Molecular Dynamics Simulation. 41st western regional American Chemical Society meeting. 10/2007.

2. The Diffusion of Small Molecules into Flavoproteins, an Enhanced Diffusion Molecular Dynamics Study. UCSD Dept. of Chemistry and Biochemistry Undergraduate Research Symposium. 5/2007.

Grants
1. Blasker Science & Technology Grant, San Diego Foundation, 2012

Professional Affiliations
American Chemical Society, 2006-present

ABSTRACT OF THE THESIS

Solution Grown Antimony Doped Zinc Oxide Films

by

Conor T. Riley

Master of Science in Chemical Engineering

University of California, San Diego, 2012

Professor Deli Wang, Chair

Zinc oxide is an extensively studied semiconducting material due to its versatile properties applicable to many technologies such as electronics, optoelectronics, sensing and renewable energy. Although zinc oxide films have been created for device fabrication, the methods used to synthesize them are expensive and unrealistic for affordable commercial devices. In addition, zinc oxide is intrinsically n-type making the realization of stable p-type materials a great challenge for light emitting diodes, solar cells and UV lasing. In this thesis zinc oxide films are created using low cost solution methods. To

accomplish this, a previously unreported surfactant, tert-butanol, is used. Several controlled experiments vary the concentration of tert-butanol, zinc and oxygen sources to demonstrate the ability of tert-butanol to create low cost films. Further, small amounts of antimony glycolate are added to the reaction solution, to create antimony doped zinc oxide films on sapphire and silicon substrates. Although hall measurements indicate that the films are n-type, a discussion of antimony activation provides a feasible path for the realization of low cost, p-type zinc oxide films.

Introduction

Zinc oxide has become an extensively studied semiconducting material due to it's large range of potential applications including light emitting diodes [1], spintronics [2], UV and gas sensing [3-6], corrosion protection [7], piezoelectronics [8-10], transparent conducting oxides [11], nanogenerators [12-14], solar energy [15-18] and photoeletrochemical cells [19,20]. However, several issues have hindered the integration of zinc oxide into commercial products. First, due to preferential axial growth, much of the recent research for low cost, low temperature solution methods have been focused on zinc oxide nanostructures such as nanowires [21], nanowalls [22], nanoflowers [23-25], nanodisks [26,27], nanopagodas [28], etc.. Although these structures may be useful in the future, their integration into modern devices have been challenging due to the costly and complicated methods required for transferring or fabricating advanced electrical contacts for compatibility. High quality films have been created using advanced techniques [29] but the cost of these methods creates an impractical expense for most commercial applications. Although films grown with low temperature wet chemical methods have been accomplished [30-32], reproducibility and film quality needs to be improved. In addition, these have mainly been accomplished on non-scalable and high cost substrates such as sapphire.

Secondly, p-type zinc oxide is a necessary component for many technologies such as LEDs, solar cells and UV lasing. Due to the intrinsic n-type nature of zinc oxide the search for stable p-type behavior remains a challenging research topic. Although p-type behavior has been observed in nano-structures [33] or by high cost methods [34] they are not commercially viable due to stability and reproducibility. Therefore, it is necessary to create a facile low cost, reproducible process for stability testing and for commercial integration.

Therefore, this thesis focuses on low cost solution grown zinc oxide thin films. To elucidate these challenges, chapter one gives a brief review of the basic structure of wurtzite zinc oxide and discusses the methods and mechanisms for morphological control. Chapter two focuses on the conduction type of native zinc oxide and surveys transition metal doping and explanations for p-type conduction. To control the axial growth of zinc oxide, tert-butanol is used. The effects and possible mechanisms of this novel surfactant are discussed in chapter three. Next, chapter four focuses on the different methods for solution film growth in the presence of tert-butanol. Finally, chapter five demonstrates the doping of antimony into the grown films and discusses the pathways for p-type conduction with this method.

Chapter 1 Low Temperature Solution Zinc Oxide Growth

Over the past decades many different methods have been used to grow zinc oxide. These include molecular beam epitaxy (MBE) [35], magnetron sputtering [36], pulsed laser deposition [37,38], metal organic chemical vapor deposition (MOCVD) [39-41] and solution growth [42-44]. Solution growth has the distinct advantage over the other processes in its facile set-up and low cost, particularly if low pressures and temperatures are used. However, due to the unique qualities of the zinc oxide crystal structure, controlling the morphology of the grown crystal presents a challenge.

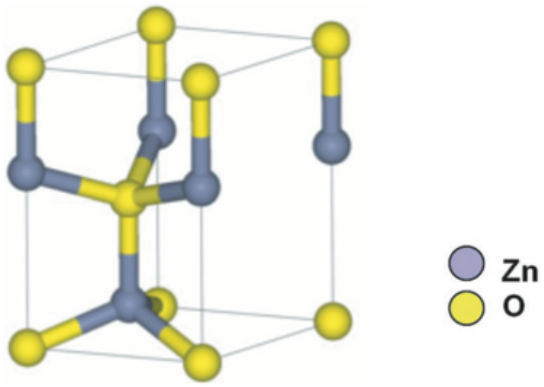

Figure 1 The wurtzite structure of zinc oxide.
Reprinted with permission from [46]

1.1 Zinc Oxide Crystal Structure

Three zinc oxide crystal structures are theoretically known to exist. This includes rock salt, zinc blende and wurtzite [45]. On the vast majority of

substrates the wurtzite structure is the most common near ambient conditions and will therefore be the crystal structure focused on in this thesis. Commonly observed wurtzite zinc oxide has a hexagonal structure with lattice parameters a = 0.3296 and c = 0.52065 nm. As seen in figure 1 this consist of alternating stacks of tetrahedrally coordinated O^{2-} and Zn^{2+} perpendicular to the c-axis.

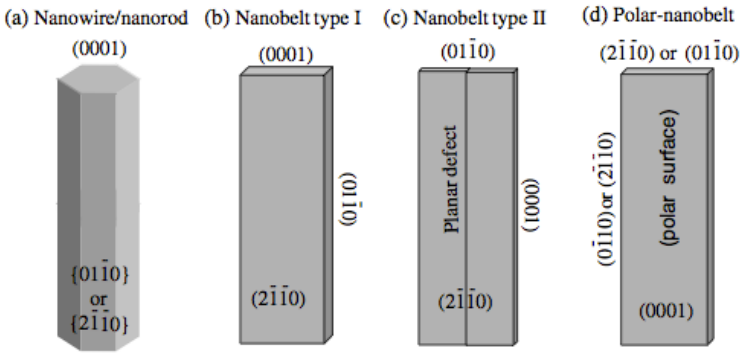

Figure 2 Commonly observed planes of wurtzite zinc oxide reprinted with permission from [47]

These alternate stacks of oppositely charged atoms give rise to a dipole moment in the direction of the c-axis creating a polar plane, (0001). The most commonly observed non-polar or lateral planes are the $(01\bar{1}0)$ and $(2\bar{1}\bar{1}0)$. Figure 2 shows these planes and the structures achieved if one of these planes dominates during the growth process.

1.2 Solution Growth Mechanism

Solution grown zinc oxide typically consists of heating an alkaline aqueous solution containing a zinc salt. If thermodynamic conditions such as concentration, temperature and pressure are satisfied, supersaturation is achieved and nucleation occurs. The direction of growth is then dictated by the minimization of free energy of the system. As described earlier, wurtzite zinc oxide has a distinct high-energy polar surface perpendicular to the c-axis. Therefore, to minimize the free energy, the monomer concentration is strongly attracted towards the polar (0001) plane, causing crystal growth to be strongly favored in the c-axis. For this reason, wires are the most commonly observed structure by solution growth. The zinc sources are usually from zinc salts such as zinc acetate or zinc nitrate. Typically, oxygen sources are either from aqueous alkaline solutions or by hexamethyltetramine (HMTA). During growth in alkaline solutions one possible mechanism is through the intermediate zinc tetrahyroxide formed by the coordination of two hydroxide groups and one zinc ion in the solution via the following reaction [48]:

$$Zn^{2+} + 2OH^{-} \rightleftharpoons Zn(OH)_2 \quad (1)$$

$$Zn(OH)_2 + 2OH^{-} \rightleftharpoons [Zn(OH)_4]^{2-} \quad (2)$$

Next, the zinc tetrahydroxide decomposes:

$$[Zn(OH)_4]^{2-} \rightarrow ZnO + H_2O + 2OH^- \quad (3)$$

Homogeneous nucleation of zinc oxide can occur via equation 3. When the zinc oxide is already present, $Zn(OH)_4^{2-}$ will decompose through reactions 4:

$$[Zn(OH)_4]^{2-} \rightleftharpoons ZnO_2^{2-} + 2H_2O \quad (4)$$

On the surface alternating stacks of zinc and oxygen are created by equations 5 and 6 [49]:

$$\{Zn^{2+}\}_{surface} + ZnO_{2,sln}^{2-} \rightarrow 2ZnO_{crystal} \quad (5)$$

$$2\{O^{2-}\}_{surface} + ZnO_{2,sln}^{2-} + H_2O \rightarrow ZnO_{crystal} + 4OH_{solution}^{-} \quad (6)$$

The point of zero charge for the (0001) plane has been observed to be at pH=8.7 [50]. At a pH higher than 8.7 the (0001) plane is negative and below 8.7 it is positive. Therefore, it is suggested that at a high pH equation 5 is sufficiently fast such that the surface is approximated as oxygen terminated and negatively charged. Conversely, at a low pH equation 6 is sufficiently fast such that the surface is approximated as zinc terminated and positively charged. This can be explained by a study [51] that showed that the main intermediates responsible for zinc oxide growth is dependent upon the pH of the reaction solution. At lower pH values positive ions such as $Zn(OH)^+$ were shown to exist

whereas at high pH values negative species such as $[Zn(OH)_4]^{2-}$ were observed. Therefore, when a charged intermediate is present the oppositely charged reaction site proceeds significantly fast such that its respective equation can be ignored. In addition, the positive or negative faces can also be explained by the adsorption of hydrogen on the surface at high pH values. This theory states that the highly polar (0001) plane will attract more negative species, requiring more protons to change signs, lowering the IEP. Conversely, the $(01\bar{1}0)$ plane will have a higher IEP than the (0001) since it does not attract negative species.

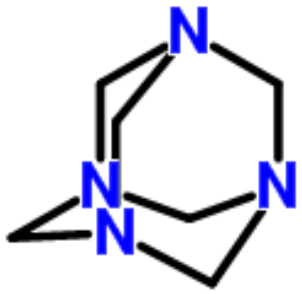

Figure 3 HMTA molecule, $(\mathbf{CH_2})_6\mathbf{N_4}$, reprinted with permission from [52]

More recently HMTA, $(\mathbf{CH_2})_6\mathbf{N_4}$, (figure 3) has been used as an oxygen source. This is a preferred reagent since it requires less attention to the sensitive changes in pH. Although its role in zinc oxide growth is controversial, it is widely thought that HMTA acts as a pH buffer by slowly providing OH^- to the zinc ions in solution. This is evident from a study [53] where it was found

that the conversion of HMTA to formaldehyde and ammonia (equation 7) has a decreased half-life from 13.8hr in a solution with a pH of 5.8 to 1.6hr in a solution with a pH of 2.0 at constant ionic strengths. The mechanism is as follows [54]: In an aqueous solution the HMTA decomposes into ammonia and formaldehyde at elevated temperatures:

$$(CH_2)_6N_4 + 6H_2O \rightarrow 6HCHO + 4NH_3 \quad (7)$$

$$NH_3 + H_2O \rightarrow NH_4^+ + OH^- \quad (8)$$

Next, the freed ammonia coordinates with the zinc ions.

$$Zn^{2+} + NH_3 \rightarrow Zn(NH_3)_4^{2+} \quad (9)$$

The thermodynamic stability of $[Zn(OH)_4]^{2-}$ is found to be significantly larger than $Zn(NH_3)_4^{2+}$ and will therefore be transformed at high pH:

$$Zn(NH_3)_4^{2+} + 4OH^- \rightarrow [Zn(OH)_4]^{2-} + 4NH_3 \quad (10)$$

$$Zn^{2+} + 4OH^- \rightarrow [Zn(OH)_4]^{2-} \quad (11)$$

As shown in Equation 11, $[Zn(OH)_4]^{2-}$ can also be formed by the hydroxyl groups formed in equation 8. Once this is accomplished zinc oxide nucleation and Ostwald ripening occur by the same process described before for alkaline

solutions. If a pH buffer is not present, a large amount of OH^- is available all at once. This will provide a large supersaturation that will create many nucleuses for crystal growth. With a pH buffer, the OH^- monomers are slowly fed to existing seeds allowing for more control and repeatability of crystal growth.

In addition to providing a basic buffered solution for zinc oxide growth, HMTA is also thought to act as a chelating agent providing further stabilization of $Zn(OH)_2$ [48]. Another theory proposes that HMTA creates a long chain polymer that serves as a surfactant to inhibit growth in the non-polar faces encouraging nanowire growth [55].

1.3 Seeded Substrates

The ability to grow well-aligned zinc oxide structures on a variety of different substrates is of particular interest to electronic devices such as LEDs, TFTs and flexible electronics. Depositing a seeding layer in combination with chemical methods has proven to be advantageous in this area [41,56-57]. To understand the mechanism of heterogeneous nucleation the equations for homogeneous nucleation must be defined.

Homogeneous nucleation occurs by the random collisions of monomers. The free energy for spherical nucleation is characterized by the sum of the volumetric free energy and the surface free energy:

$$\Delta G = -\frac{4}{3}\pi r^3 G_v + 4\pi r^2 \sigma \quad (12)$$

Where σ is the surface tension, r is the radius of the particle, and G_v is the volumetric free energy.

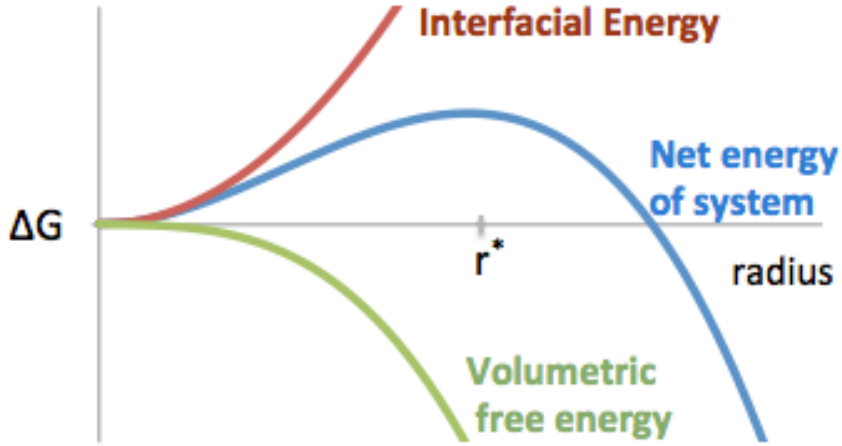

Figure 4 Free energy of homogenous nucleation

Equation 12 is a linear superposition of the free energy for bulk and surface formation. Since it costs energy to form a surface, an initial energy barrier must be overcome to achieve spontaneous growth, as illustrated in figure 4. When enough energy is achieved, $\frac{d\Delta G}{dr} = 0$. Here, a threshold value of r is reached known as the critical radius:

$$r^* = -\frac{2\sigma}{G_v} \quad (13)$$

Above this radius spontaneous growth occurs via Ostwald ripening.

On the contrary, heterogeneous nucleation occurs when a solid surface is present in the solution and acts as a catalyst for nucleation by allowing the monomers to be in close proximity, reducing the energy barrier of nucleation [58]. In the case of seeded substrates the nucleation process is bypassed allowing for a lower level of supersaturation required for crystal growth [48].

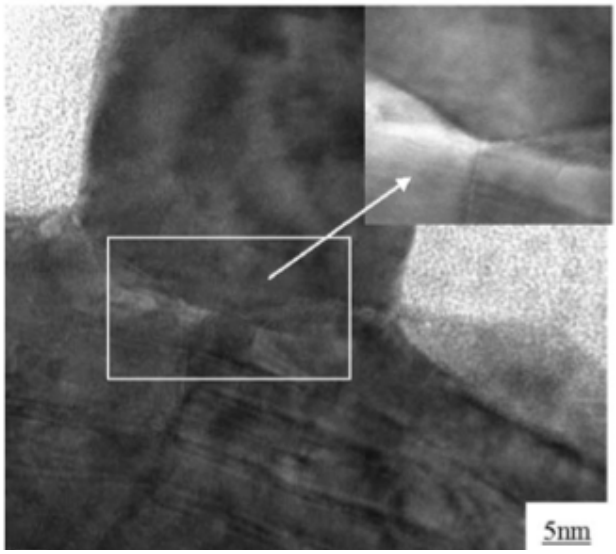

Figure 5 TEM image of zinc oxide nanowire growth from the concave tip of the zinc oxide seeding layer grain. Reprinted with permission from [64]

Seeding the substrate for zinc oxide growth has been accomplished in a few different ways. The most common methods include oxidizing zinc metal [59], spin coating zinc oxide nanoparticles and RF magnetron sputtering [60-62]. The conditions of seeding layer deposition and the type of substrate can

have a large impact on the crystal growth in terms of homogeneity, density, orientation and diameter of the nanowires. In one study [63] the authors deposited a zinc oxide layer by sputtering and increased the grain size by annealing at 600˚C and 800˚C. It was found that the diameter of the nanowires increased when the grains in the seeding layer were larger. TEM images revealed that the nanowires grew at the concave edges of each grain where the surface energy is largest [64]. This is shown in figure 5 where close examination reveals parallel lattice fringes connecting the nanowire and the concave tip of the seeding layer grains. Another study varied the thicknesses of a sputtered zinc oxide seeding layers and found the density of nanowires were greatly reduced when the thickness was less than 4.0nm [65]. The authors observed that thin seeding layers created islands that led to less nucleation sites for nanowire growth. Once a critical thickness was reached (between 5 and 50nm) only small changes in nanowire properties were observed.

1.4 Surfactants and manipulation of zinc oxide growth

Manipulating the morphology of zinc oxide nanostructures has been the subject of many research projects. Wet chemical morphology manipulation presents additional obstacles since the system is always in thermodynamic equilibrium. For this reason growth in the (0001) plane is favored, making nanowires the most pervasive structures created by wet chemical methods.

Therefore, in order to selectively control the morphology of zinc oxide, certain measures must be taken. Typically this is accomplished by adding a surfactant that selectively binds to one crystal face, blocking its further growth, and allowing growth to continue on the unselected face. In order to accomplish this each of the crystal faces must have different electrostatic properties. Since the charge of the zinc oxide is dependent on surface states, the pH of the solution plays a crucial role. The majority of publications site the isoelectic point (IEP) of zinc powder as being the pH where the $(01\bar{1}0)$ plane changes signs leaving a range at which the (0001) plane may be oppositely charged. However, this may not be a good choice since the IEP indicates when a zinc oxide particle becomes oppositely charge due to proton adsorption. However, wurtzite zinc oxide is anisotropic and therefore the (0001) and $(01\bar{1}0)$ planes have very different properties than a zinc oxide particle. For this reason many different IEP values have been reported for zinc oxide, ranging from 7.2 to 10.3 with the majority of publications using the value of 9.5 [60-62]. Therefore rigorous tests must be done to determine the charge of the crystal faces at a given pH. This has been accomplished at pH values close to 11 [69,70].

Several organic surfactants such as the citrate, polyethylenimine (PEI) and ethylenediamine (EN) have been shown to exhibit this behavior [65,66,69]. EN and PEI possess amine groups that stay protonated at a pH over 10 and are thus positive. When PEI or EN is added to the solution at pH>10, it is thought to selectively bind to the $(01\bar{1}0)$ plane blocking lateral growth, allowing

Ostwald ripening to proceed faster in the c-axis, creating high aspect ratio nanowires. In contrast, negatively charged carboxyl and alcohol groups containing molecules, such as sodium citrate, can selectively adsorb to the (0001) plane inhibiting growth in the c-axis, creating low-aspect ratio nanowires or nanodisks. In addition to organic compounds, adjusting the aspect ratios of nanowires has been demonstrated by inorganic salts [70]. Here, the authors found that certain types of metals created differently charged complexes at pH=11, hindering growth of the respective face. Many other nano-structures have been created such as nano-belts [71,72], twinning [73], nanotubes [74-76], nanorings [77] and hierarchical [78,79] using novel processes to further exploit the unique qualities of solution grown wurtzite zinc oxide.

1.5 Film growth

Of particular interest to electronic devices are films. Having high quality films eliminates the need for the complicated contacts and/or transfer steps, significantly decreasing the cost of device fabrication. Solution grown films of good quality are created when well-aligned nanowires are cemented together by a process known as “oriented alignment” [80]. To accomplish this, the seeding layer must completely cover the substrate and allow the nanowires to be well-aligned. After the seeding layer is deposited, films are grown in two ways. If the seeding layer allows for perfect c-axis orientation, long periods of growth time can create very high film qualities [30]. However, this process is

very sensitive to small changes in deposition and thus repeatability has been found to be low. Another method has been shown to accomplish films by renewing the reaction solution. First, the nanowires are grown by common methods. Next, the nanowires are removed from the reactor, cleaned and added to a new reactor containing a fresh monomer concentration and a c-axis inhibiting surfactant. In the presence of the surfactant the nanowires grow into each other during the subsequent growths. After the second or third growth films are observed [31,32].

Chapter 2 Zinc Oxide Doping

Another way to change the physical properties of semiconductors such as zinc oxide is by slightly changing the composition by incorporating or "doping" small amounts of metal into the crystal structure. In addition to improving conductivity and changing conductivity type this process has proven to be useful in improving other areas such as ferromagnetism [81] and band gap tuning [82,83]. This thesis will focus on doping elements that aim to change the conductivity type of zinc oxide.

Semiconducting materials are categorized as materials that have conductivity between metals and insulators. Thus, semiconductors have band gaps that are large enough allow electrons to be promoted to the conduction band only by overcoming a barrier with addition energy such as heat.

Replacing the host atom with an atom that has one more electron in its valance creates an extra electron that is not tightly bound. This extra electron increases the electron donating behavior; negative conductivity (n-type). Conversely, replacing the host atom with an atom that has one less electron in its valance creates a deficit of electrons (increase of holes). The addition of holes increases the electron accepting behavior, positive conductivity (p-type). In materials such as silicon, where only one element exists, doping is relatively straightforward. In materials such as zinc oxide, where two sites exist, doping

becomes more complicated since the dopants have the ability to either replace a zinc or oxygen sites.

2.1 N-type zinc oxide

Undoped wurtzite zinc oxide has been found to be intrinsically n-type [84]. Although the mechanism has been the subject of much debate, many argue that the donor concentration is mainly due to oxygen vacancies and zinc interstitials [85,86]. However, it has been argued that oxygen vacancies act as deep donors and zinc interstitials have too high of a formation energy and therefore cannot contribute to the electron density in the conduction band [88]. Another argument has been given for hydrogen doping. Hydrogen can take on two states: H^+, which has been shown to be donating, and H^-, which has been shown to be accepting. In the vast majority of semiconductors both states are present and do not contribute to the overall conduction type of the material. However, in zinc oxide only the donating state has been found to be stable, adding to its n-type conductivity [87,88]. To further increase the n-type conductivity of zinc oxide, aluminum has been doped into the crystal structure by many methods including solution growth [89].

2.2 P-type doping

Due to the intrinsic n-type characteristics of zinc oxide, the creation of p-type materials has been a challenge. To overcome these obstacles various

doping elements have been used such as, lithium [90], sodium [91,92], potassium [80,93], nitrogen [94], silver [95], phosphorus [96-99], arsenic [100,101] and antimony [102-104]. Since dopant concentration solubility increases with temperature, methods such as chemical vapor deposition have been widely used. Recently, lower cost solution methods have shown some success. In particular electrochemical doping of silver into zinc oxide nanowires has been realized using an electrochemical-solution approach [95]. However, some promising results come from antimony doping by the solution growth method [102,104]. In this work the authors use antimony glycolate as the doping agent. As illustrated in figure 6, they theorize that the chelating ligands enable the antimony to be slowly fed into the zinc oxide matrix much like HMTA slowly feeding OH^- to the growing nanostructures. Any effort to use wet chemical methods to dope antimony into nanowires has not been accomplished without the glycolate ligand.

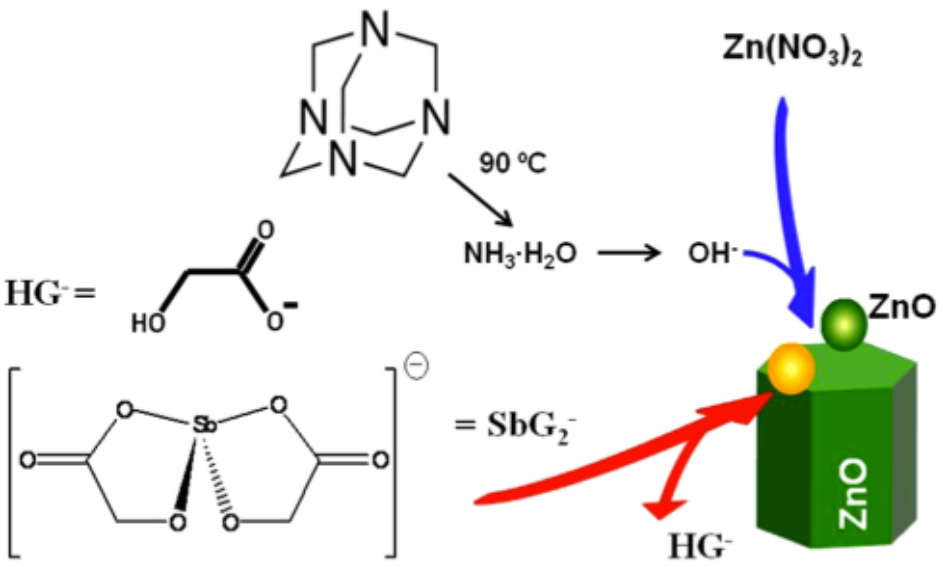

Figure 6 Molecular structure of antimony glycolate and antimony doping mechanism. Reprinted with permission from [102].

The doping mechanism of antimony has caused some controversy. It was originally thought that pnictogens would have to replace oxygen in order to have p-type conductivity. However, the atomic radius of arsenic (1.20Å) and antimony (1.40Å) are large compared to oxygen (0.73Å). Theoretically, this would cause too much strain on the crystal structure. In an effort to explain this phenomena calculations determined that the Sb_{Zn}-$2V_{Zn}$ complex would cause p-type conduction and is likely to be the culprit due to a low formation energy relative to the other possible defects [105]. However, this still remains a controversial research topic [106].

Chapter 3 Tert-butanol as a Surfactant

To reliably make solution grown zinc oxide films, a surfactant that increases the lateral growth is required. As described in chapter one of this thesis, the only known surfactants capable of achieving films by inhibiting axial growth are sodium citrate, cadmium, copper, magnesium and calcium ions. Unfortunately the existence of these small ions has been reported as dopants and can contaminate the film.

Therefore, it is important to realize a new surfactant. In this thesis the surfactant of interest is tertiary butanol. Tertiary butanol (t-butanol) is one of the four possible butanol isomers. Due to the electron withdrawing properties of tertiary carbons, the hydroxyl group is stabilized giving it a high pKa value of 19. T-butanol forms a positive azeotrope in water giving the mixture a boiling point of 79.9˚C [108]. The following experiments are used to demonstrate the ability of t-butanol to inhibit zinc oxide growth on the (0001) plane.

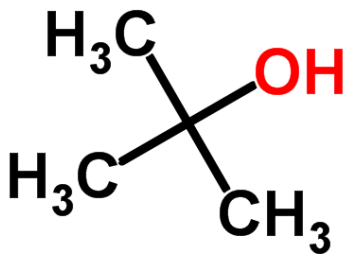

Figure 7 Tert-butanol molecule reprinted with permission from [108]

3.1 Experimental

In order to assess the ability of t-butanol to suppress the growth in the (0001) plane the following procedure was followed. First, phosphorus doped silicon was obtained, cut into 1cm^2 squares and taken to a class 1000 cleanroom. Next, it was cleaned with 1.6M nitric acid in deionized water. The samples were then rinsed with deionized water and subsequently sonicated in a 1:1:1 mixture of isopropanol, acetone and deionized water. The samples were then rinsed with deionized water and blown dry with nitrogen. Next, a thin film of zinc oxide was applied to the cleaned substrates with the Denton Discovery 18 Sputtering System. The base pressure was 2.1×10^{-6} mT. To eliminate any organics left on the substrate, a gentle argon etching was applied to the substrates by applying a 200W RF bias to the stage and with a 2.1mT active pressure of argon for 45 seconds. Next, a 200W RF bias was applied to the zinc oxide target at 2.5mT of argon. The shutter was left closed with the power on for five minutes to clean off any contamination on the surface of the target. Then, the shutter was open for 10 minutes. The zinc oxide deposition rate was determined to be 4nm/minute. The thickness was determined to be 40nm with a Dektak 150 stylus surface profiling system. The samples were then taken out of the clean room and adhered to a glass slide such that the seeding layer side was exposed. A solution of 10mM zinc acetate and 10mM HMTA in deionized water and/or t-butanol was prepared. The total volume of the solution was 30ml with the volume of t-butanol varying from 0ml to 29ml.

The samples were then placed in a 100ml three-neck flask such that they were facing downwards. Subsequently, the solution and a stir bar were poured into the flask. One of the necks was covered with parafilm, the other was used to monitor the temperature with a thermometer and the third was connected to a reflux column to prevent solution evaporation. The flask was then lowered into an oil bath, under gentle agitation and heated to 75˚C. Once the sample reached around 60˚C the solution turned whitish. After 2hrs the samples were removed from the solution, rinsed with deionized water and blown dry with nitrogen. The samples were then characterized with a Phillips XL30 scanning electron microscope at 10kV and a working distance of 10mm. Diameters of the nanowires were determined by selecting a square within the SEM image with an area equal to twice the scale bar squared. Within that square the diameter of each nanowire was measure with a ruler. The average diameter was then calculated and used as the reported value. Length/film thicknesses were determined by inspection of SEM images with a ruler. In order to examine the structures of homogeneously grown crystals, small amounts of the reaction solution were dropped onto a small silicon square after each growth and dried on a hotplate at 110˚C before being examined by SEM.

3.2 Results and Discussion

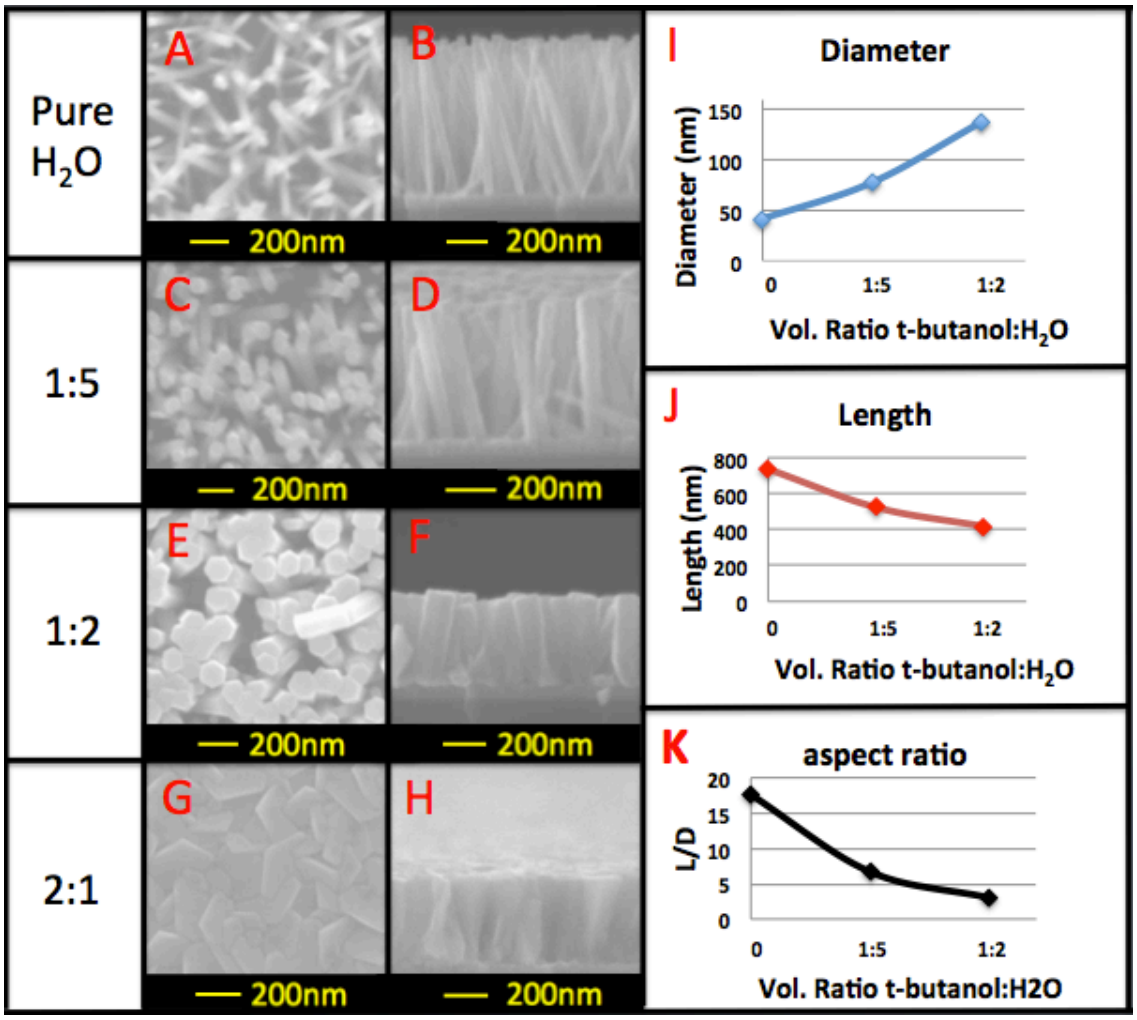

Figure 8 SEM images of nanowire and film growth with increasing t-butanol:water volumetric ratios (a-h), graphs displaying the effects of increasing tert-butanol concentrations on the nanowire diameters (i) lengths (j) and aspect ratios (k)

As illustrated in figure 8, increasing the t-butanol:H_2O volumetric ratio dramatically increases the diameter and decreases the length of the nanowires.

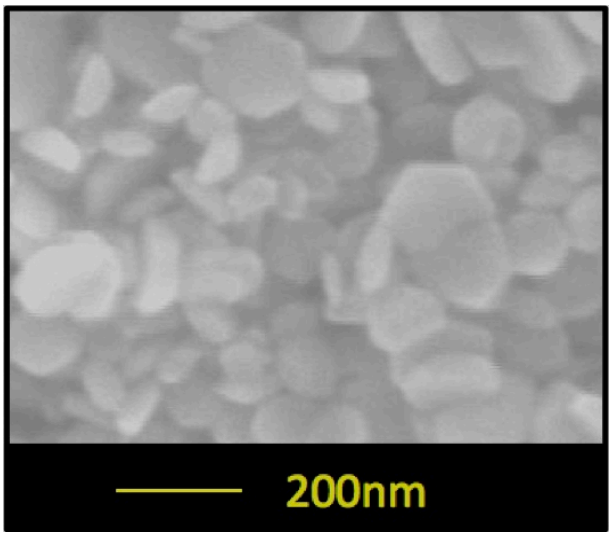

Figure 9 Homogenously grown nano-disks in solvents containing a 29:1 volumetric ratio of tert-butanol:water

This allows for the aspect ratios of the nanowires to be adjusted by a factor of six. Between a volumetric ratio of 1:2 and 2:1 the nanowires converge, creating a film. When the concentration of t-butanol is increased to 29:1, heterogeneous nucleation does not occur. Instead the solution turns a solid white from the presence of homogeneously nucleated zinc oxide nanodisks, as shown in figure 9.

The pH of the reaction solution without t-butanol varies between 7 and 7.3. The addition of t-butanol decreases the pH to 6.6. Both values are below the isoelectric point of zinc oxide. It is clear from a previous study [50] that the (0001) face is positive at this pH. However, the charge on the $(01\bar{1}0)$ at this pH has not been identified. It is therefore possible that the tertiary alcohol on t-butanol selectively binds to the positively charged (0001) plane while the $(01\bar{1}0)$ plane stays relatively uncharged and unaffected by the t-butanol. This is most drastically seen in the growth solution containing a 29:1 t-butanol:water concentration where nanodisks are formed. Here, homogeneous nucleation is favored and the t-butanol forms micelles around the forming crystals, inhibiting axial growth. This has been observed in other studies with small amounts of emulsifiers [110,111]. In addition to selective adsorbing to the (0001) plane, t-butanol also lowers the pH of the solution which can also change the reaction rate and morphology of zinc oxide structures [111]. However, only modest changes (1.5 fold change) in the aspect ratio have been observed by adjusting the pH. In order to fully understand the c-axis inhibiting properties of t-butanol more tests must be carried out to determine the complexes formed and the surfaces charges of the crystal faces in these solutions.

Chapter 4 film growth with t-butanol

The purpose of the experiments in chapter three was to examine the aspect ratio of the nanowires thereby evaluating the ability of t-butanol to inhibit growth in the axial direction. To accomplish this, low molar concentrations of the zinc and oxygen sources were used. This was done since it was observed that at higher concentrations films were created with t-butanol, making it difficult to examine the surfactant properties.

In this chapter the principles from chapter three are used to grow zinc oxide films. The films are grown with t-butanol using two methods. The first method uses the same procedure outlined in 3.1 except the solution volume was fixed with a 1:2 t-butanol:water volumetric ratio. In addition, the growth time was decreased to 1hr and the HMTA and zinc acetate concentration was varied from 5mM to 25mM.

4.1 Method 1 - Single solution growth

As seen in figure 10a-j, the nanowires begin to converge around 15mM concentrations. In addition, the diameter of the nanowires increases from 5mM to 20mM. By 20mM the nanowires have completely converged, creating a film. At the highest concentration of 25mM, the diameters of the nanowires

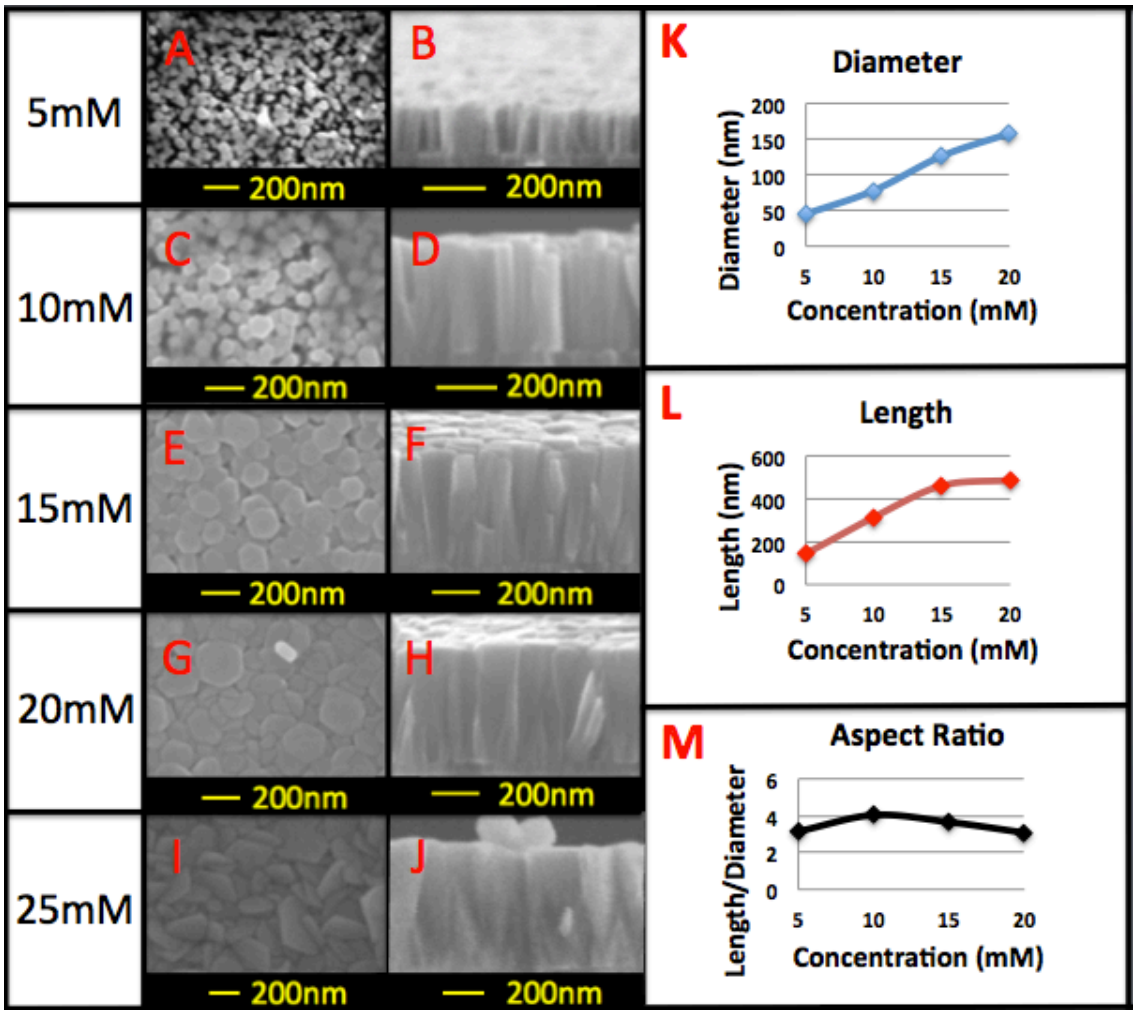

Figure 10 SEM images of nanowires and films grown with varying zinc acetate and HMTA concentrations (a-j) graphs describing the effects of reagent concentration on nanowire diameters (k), length (l) and aspect ratios (m).

become impossible to calculate since they to grow into each other, disrupting vertical alignment. The length of the nanowires increases significantly from 5mM to 15mM. Above this concentration the length increase is relatively small. Figure 10d shows the aspect ratios for the different concentrations. The aspect ratio ranges from 3.08 to 4.03. For the most part, the aspect ratio of the wires stays relatively constant with varying concentrations. However, a slight trend is

present. A logical explanation for this observation is as follows. At higher concentrations monomers completely cover the highly polar (0001) surfaces, making them more neutral so that the remaining monomers are attracted to the $(01\bar{1}0)$ surfaces allowing for increased lateral growth. At lower concentrations growth is more competitive and the diminishing monomers are more concentrated toward the polar surfaces. However, at concentrations lower than 5mM minimum diameters must be achieved in order to minimize the surface energy of the concave grain tips. Once this diameter is achieved only a small amount of monomers are left to grow the wires vertically, leaving the aspect ratio low.

Although more monomers are present at higher concentrations, the film thickness is only slightly changed from 15mM to 25mM. Essentially, less material per added reactant is being deposited on to the substrate. This is most likely due to increased homogeneous nucleation occurring in the solution at higher concentrations. This theory is corroborated by the observation of increased precipitates as the concentration is increased. Homogeneous nucleation is more likely to occur at higher concentrations since larger supersaturation values are obtained, increasing the energy of the system needed to overcome the barrier for not only heterogeneous nucleation but homogeneous nucleation as well.

As seen in figure 10a-j, poor quality films are created using a 25mM solution of zinc acetate and HMTA in a 1:2 t-butanol:water volumetric ratio. In

order to increase the quality of the films, longer growth times were used. It was found that 15-hour durations provided improved film properties as shown in figure 11. This 15 hour growth is what will be referred to as method 1 in this thesis (table 1).

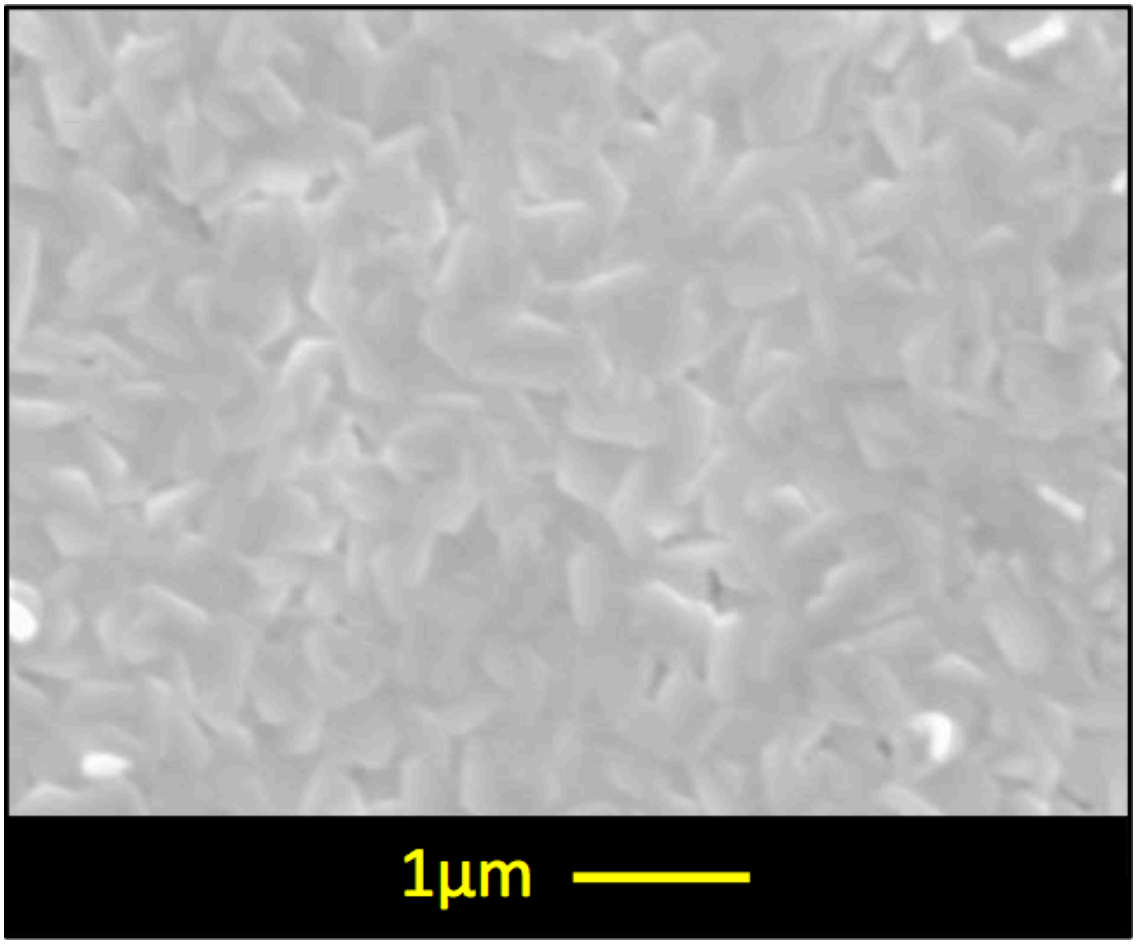

Figure 11 Zinc oxide film with 15-hour reaction time, 25mM reagent concentration and 1:2 t-butanol:water volumetric ratio (Method 1)

4.2 Method 2 - Multiple solution growth

The second method of zinc oxide film growth explored in this thesis involves renewing the reaction solution. In this method the substrates and reaction set-up are the same as in section 3.1. As specified in table 1, the duration of each growth is 1hr and the reaction solutions contain 25mM concentrations of zinc acetate and HMTA. The first reaction has a 1:11 t-butanol:water volumetric ratio. The volumetric ratio is increased to 1:5 for the second growth and the third growth to 1:2. In between reactions the samples are then taken out, rinsed with deionized water and put in a clean reaction vessel.

As seen in figure 12 the first growth provides nanowires. The subsequent growths create films by allowing the nanowires to grow laterally and converge. By the third growth the nanowires are completely merged and the film is complete.

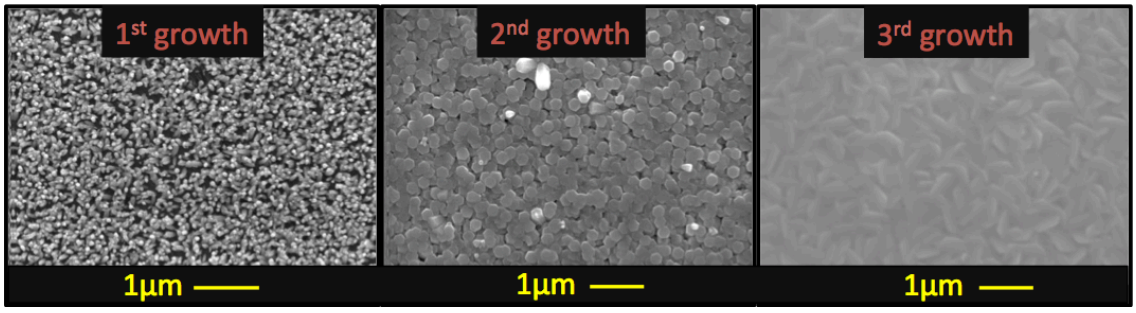

Figure 12 Three-step method (method 2) for growing zinc oxide films

Figures 11 and 12 both show the creation of films by two different methods. Although good film coverage is accomplished, the surface seems to be rough for both. By examining the cross section of the films and nanowires, it can be seen that perfect axial alignment is not achieved. This causes the wires to grow into each other causing the edges to protrude out of the films. This is most likely due to seeding layer deposition conditions. Hence, it might be possible to minimize the surface roughness by adjusting the seeding layer deposition conditions. Doing so could lead to improved electrical and optical properties of the films.

Table 1 Summary of film growth methods

		Method 1	**Method 2**
Reaction 1	t-butanol:H2O (vol. ratio)	1:2	1:11
	Time (hr)	15	1
	Precursor concentration (mM)	25	25
Reaction 2	t-butanol:H2O (vol. ratio)	-	1:5
	Time (hr)	-	1
	Precursor concentration (mM)	-	25
Reaction 3	t-butanol:H2O (vol. ratio)	-	1:2
	Time (hr)	-	1
	Precursor concentration (mM)	-	25

Chapter 5 Antimony Doped films

In efforts to create UV emitters and high energy LEDs, stable p-type zinc oxide films are desirable. In this thesis antimony is used since recent publications [102-104] support its use as a p-type dopant for zinc oxide. To accomplish this, the methods for antimony doped nanowires are adapted from literature [102] and combined with the film growth methods described in chapter four.

5.1 Experimental

35-40nm zinc oxide seeding layers are deposited by RF magnetron sputtering to silicon and c-sapphire substrates by the same process described in section 3.1. First, the dopant solution (1) is made by mixing equimolar solutions of sodium hydroxide and glycolic acid in deionized water to make sodium glycolate. Next, antimony(III) acetate is added such that the molar ratio of antimony to glycolate is 1:12. Shortly after, an equimolar solution of zinc acetate and HMTA is created (2). Next, solution (1) is added to solution (2) such that the antimony to zinc ratio is 2:100. Next, the t-butanol is added to the solution and stirred. The total solution volume is 30ml. The substrates are adhered to the glass slide and placed faced down in a 100ml three-neck beaker. The solution is poured into the reaction vessel with a stir bar connected to a reflux column and thermometer. The third neck is sealed with

parafilm. The solution is then heated to 75˚C. The duration times and t-butanol volumes used are the same as outlined for both methods. In an attempt to activate the antimony in the zinc oxide, the substrates are annealed in a tube furnace at 850˚C in air for 30 minutes. A slow cool down rate of 5.5˚C/minute is used to prevent film cracking. Efforts to create ohmic contacts consisted of depositing 30nm of NiO and 500nm of Au to the four corners of the square substrates by RF magnetron sputtering. The substrates with contacts are then annealed using rapid thermal annealing at 800˚C for 120s under N_2 with an AG Associates Heat Pulse 610. The ohmic character of the contacts was assessed with a home built probe station set up to a Keithly ammeter and National Instruments voltage source between 5 and -5V. Each of the four contacts was tested. Hall measurements were done on a home-built set-up using the van der Pauw method performed at room temperature. Using this set-up film resistivity, carrier concentration, mobility and conduction type, were determined for the silicon and sapphire samples for method 1 and the silicon sample for method 2. The morphology of the films was examined using SEM imaging as described in section 3.1. The EDX measurements were done using an Oxford EDX unit attached to the Phillips XL30 ESEM. X-ray spectra analysis was performed using Inca software. AFM images are taken with a Veeco scanning probe microscope equipped with a standard silicon probe (Umasch NSC15) in tapping mode. Surface roughness and grain size were determined with nanoscope analysis software. Ex situ XPS measurements of the O 1s and Sb $3d_{3/2}$ levels

were performed on the silicon and c-sapphire samples for method 2 after annealing. XPS measurements were conducted at Beijing electron spectrum center lab (Tsinghua University, Beijing China), equipped with Al Kα source at 25 W. The base pressure of the analysis chamber was $4.5x10^{-10}$ mTorr. The binding energy scale was calibrated to the carbon line at 284.8eV. All XPS spectra were recorded with a resolution of 0.51μeV. Each data set was first corrected for the non-linear emission background. The data was then fitted with a Gaussian function to find the peak positions.

5.2 Results

Figures 13a-c indicates that films have been accomplished with these methods. The morphology of these films is similar to the films grown in chapter four. This indicates that the dopant solution has little effect on the ability of t-butanol to inhibit axial growth and create films. By inspection of the SEM images, annealing seems to have a slight effect on the films by smoothing out the edges and slightly increasing the grain size. The difference in the grain size between the films grown on c-sapphire and silicon can be attributed to the difference in the lattice mismatch. Specifically, c-sapphire and zinc oxide have a lattice mismatch of 31% [112] whereas silicon and zinc oxide have a lattice mismatch of 39% [113]. In general, decreasing the lattice mismatch between

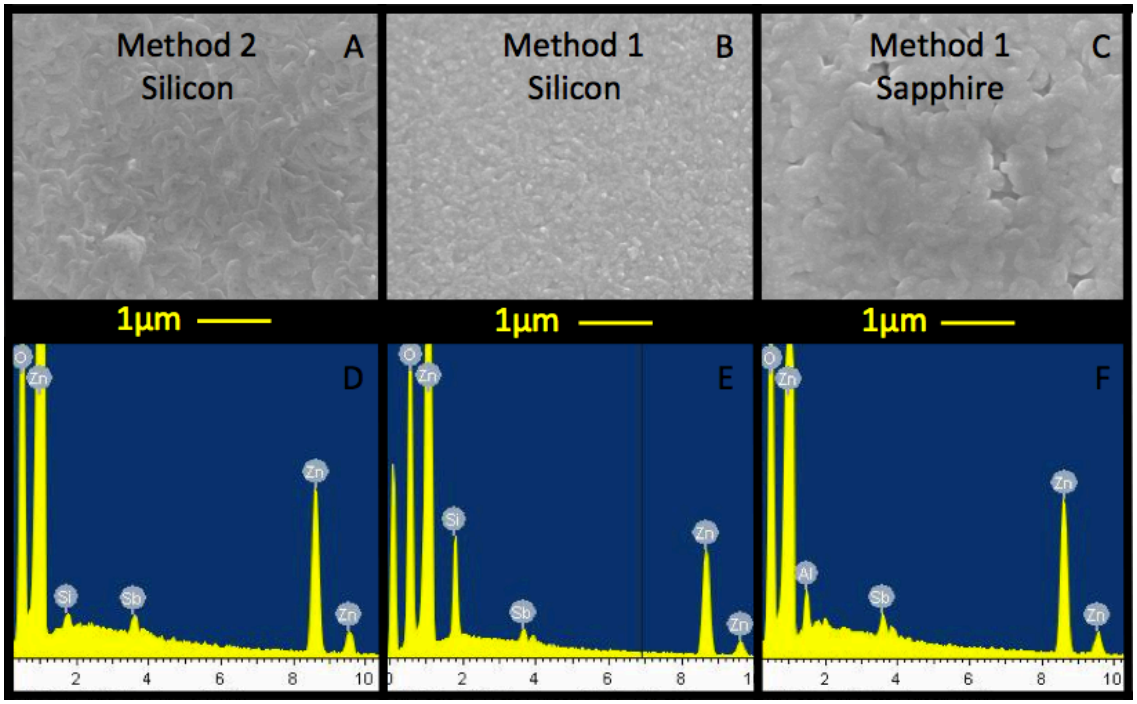

Figure 13 SEM images of antimony doped zinc oxide films grown by different methods (a-c) EDX measurements of respective samples (d-f)

two materials increases the crystallinity (larger grain size) of the sputtered film. This is consistent with reports for zinc oxide on sapphire and silicon [114].

As seen in figure 14 the film thicknesses for methods 1 and 2 are 750nm and 1000nm, respectively. Although the film in method 1 is exposed to the monomers for a longer time, the film in method 2 is thicker. This is because method 2 exposes the film to a new reaction solution three times. At the beginning of each of these reactions the monomer concentration is the largest and therefore the reaction rate is at its fastest. Therefore, renewing the reaction solution three times exposes the crystal surface to more monomers than a 15-hour growth.

Figures 13d-f show the EDX spectrums for the antimony doped zinc oxide films. Here, the peaks at 3.6 keV clearly show the existence of the antimony. The elemental analysis in EDX measurements is thought to be only for qualitative analysis. However, each of the films was calculated to contain around 0.8 at% antimony relative to zinc oxide. This finding is in accord with other publications [102]. Further, none of the films grown without antimony exhibited this peak.

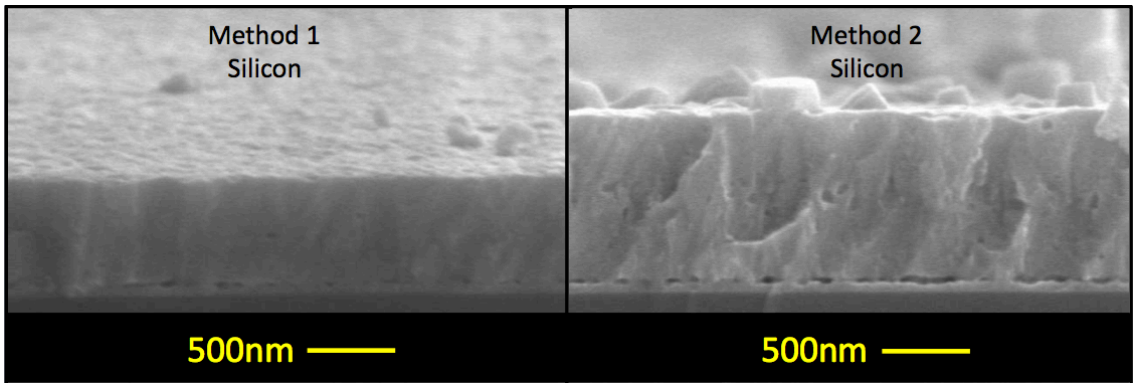

Figure 14 Cross sectional view of antimony doped zinc oxide SEM images

In addition, figure 15 clearly shows peaks for the O 1s and Sb $3d_{3/2}$ levels in XPS measurements. The existence of the Sb $3d_{3/2}$ near 540eV has been reported to represent antimony oxide, indicating that the antimony has likely doped into the zinc sites [104,115]. Further, the oxygen peak has been deconvoluted into two peaks. This is due to the different oxygen states present

for solution grown zinc oxide films. Since XPS only probes the surface of the sample, the oxygen is present in three forms as H_2O, Zn-OH and Zn-O. These peaks have been reported to be at 532.9eV-533.3eV, 531.9eV and 530.5eV, respectively [116,117]. Therefore, the furthest down-field peak within the O 1s level is attributed to zinc oxide in the crystal whereas the up-field peaks are attributed to oxygen present in adsorbed water and bonded hydroxyl groups. Further, no sodium peaks were present in the XPS data indicating that only the antimony ion was doped into the film.

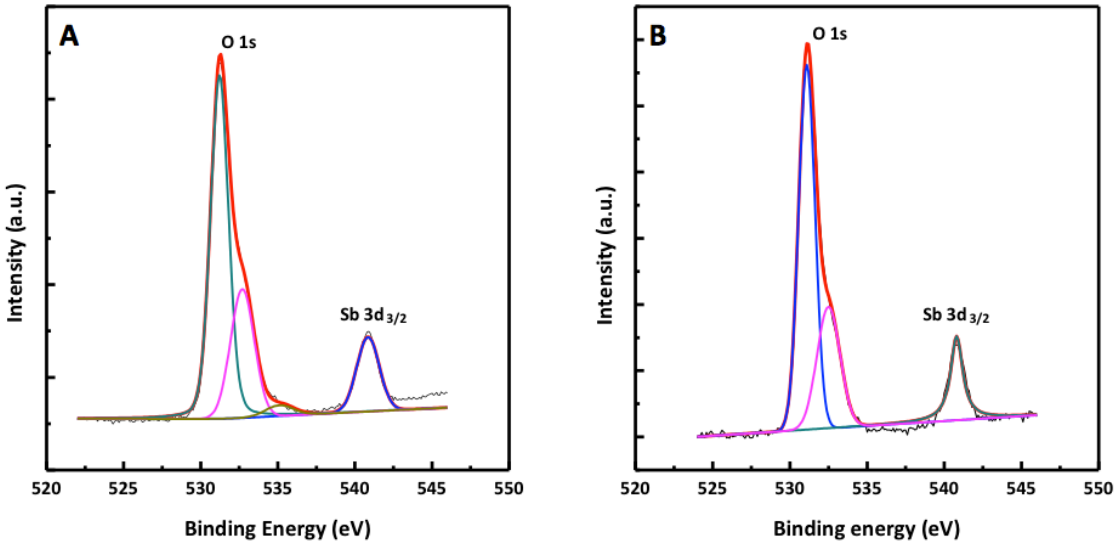

Figure 15 XPS of antimony doped zinc oxide films on sapphire (a) and silicon (b) by method 1

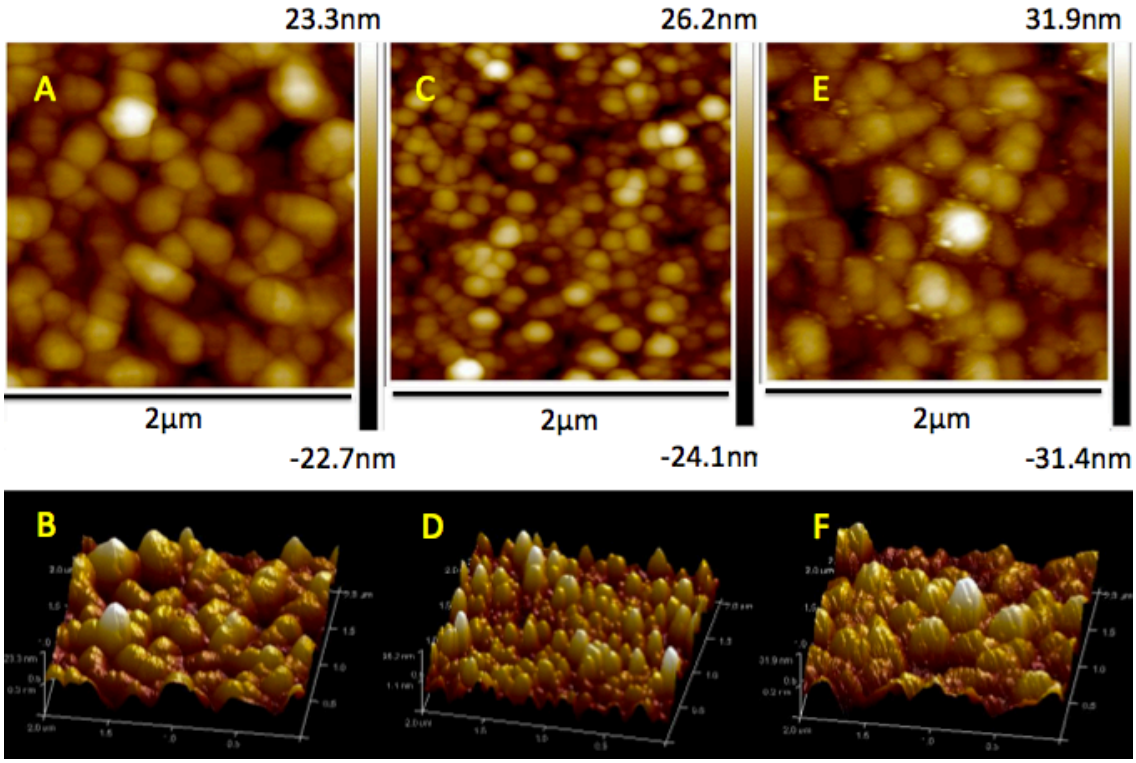

Figure 16 2D and 3D images of method 2 on silicon (a,b), method 1 on silicon (c,d) and method 1 on sapphire (e,f) by AFM

Atomic force microscope (AFM) images are given in figure 16. By comparing the results from figure 16 and table 1 on silicon it appears that the grain size is significantly larger by method 1 than method 2. This is consistent with figures 11 and 12. This implies that the grains increase in diameter fastest during the first hour of growth. Since method 1 repeats the first hour of growth three times it's diameter is larger whereas method 2 samples are only exposed to fresh monomer concentrations once. Despite the differences in the methods the surface roughness of the samples are similar.

Table 2 AFM Analysis

AFM Analysis	Avg. Grain Size (nm)	RMS Surface Roughness (nm)
Method 2 Silicon	240	8.17
Method 1 Silicon	129	8.57
Method 1 Sapphire	130	9.51

Figure 17 shows that ohmic contacts were accomplished by method 1 on sapphire and silicon. Interestingly, despite having the similar compositions, method 2 on silicon showed very different properties. As shown, this sample displays a Schottky barrier between the contacts and the sample. Since ohmic contacts were not achieved, Hall measurements were deemed inconclusive for this sample.

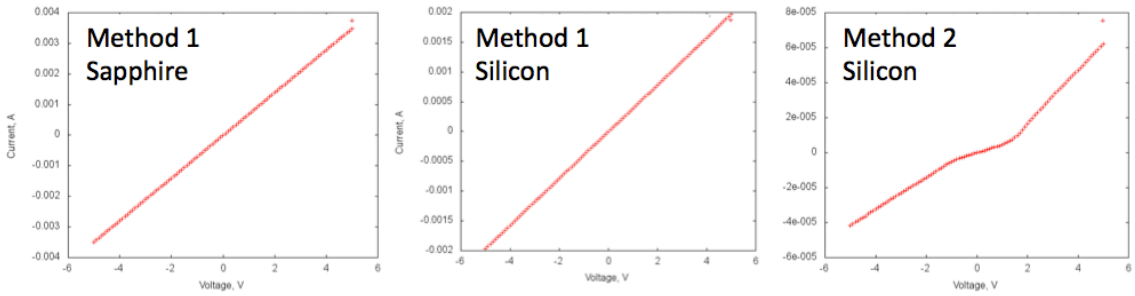

Figure 17 IV plots testing the NiO/Au contacts sputtered onto the antimony doped zinc oxide films. Ohmic behavior is observed by method 1 and a Schottky barrier by method 2

Table 2 summarizes the results of the Hall measurements for the surviving samples. Despite antimony doping, the films did not show p-type character. However, highly conductive n-type films are created due to high mobilities, and elevated carrier concentrations.

Table 3 Hall measurements

Hall Measurements	**Method 1 Sapphire**	**Method 1 Silicon**	**Method 2 Silicon**
Conductivity type	n	n	inconclusive
Carrier concentration (cm^{-3})	1.64E+19	1.07E+19	inconclusive
mobility (cm^2/Vs)	2.58	2.48	inconclusive
resisitivity (ohm-cm)	0.08838	0.1407	inconclusive

Creating stable p-type zinc oxide is a challenge because this typically consists of three steps, integrating dopants into the zinc oxide matrix, activating the dopants and eliminating point defects that that cause electron donation. As demonstrated, the first step has been accomplished, however, the elimination of point defects and activation of antimony is highly dependent on annealing conditions. This behavior has been observed with potassium doped zinc oxide [32]. Here, the authors observed the conductivity type to switch from n to p by varying the annealing conditions. This was attributed to the activation and desorption of hydrogen defects, which is in accord with stability testing of ion-implanted hydrogen research in zinc oxide [118]. In order to create p-type zinc oxide by solution growth many different annealing conditions must be tried. In

addition, the observation that ohmic contacts are accomplished with method 1 but not method 2 indicates that the two materials may have different properties such as work functions and perhaps conductivity type. Also, significantly less conductance of method 2 could be a result of more p-type character since n-type materials typically display higher mobilities like the ones shown in the Hall measurements. More tests must be done to determine the difference in the films.

Conclusions

The purpose of this research was to create low cost films on abundant substrates and to demonstrate the ability of antimony doping. As discussed in chapters three and four, decent quality films are prepared and characterized using t-butanol as a surfactant. This finding provides, not only an inexpensive method for zinc oxide film deposition but also provides a reliable surfactant without adding any possibility of contamination from anions as in the sodium citrate currently used for solution growth of zinc oxide films. Chapter five shows that this method is compatible with previously reported doping methods by incorporating antimony into the films.

The future work for this method will be aimed at realizing p-type materials by trying different annealing conditions. In addition, different contacts must be tried in order to get ohmic contacts for films grown by method 2. Further, it must be determined if the high conductivity of the films grown by method 1 is due to the antimony or point defects. For comparison, films without antimony doping will be tested using Hall measurements, XPS and AFM. Also, the doping of additional transition metals could increase n-type conductivity and create a low cost method for creating a transparent conducting oxide.

The sputtered seeding layer was used due to its homogeneous films growing properties. Films were grown with solution methods, however, complications ensued due to non-uniform coverage and were therefore not

discussed in this thesis. Once the films are determined to have the desired characteristics, it is entirely possible to replace the sputtered seeding layer with a solution grown seeding layer. Once accomplished, the films will be highly inexpensive and scalable with a set-up that can be created with little effort.

Bibliography

[1] Park, W. I.; Yi, G. C,; Electroluminescence in n-ZnO Nanorod Arrays Vertically Grown on p-GaN, Adv. Mater. 2004, 16, 87-90

[2] Opel, M,; Spintronic oxides grown by laser-MBE, J. Phys. D: Appl. Phys. 2012 ,45, 033001

[3] Wei, T. Y.; Yeh, P. H.; Lu, S. Y.; Wang, Z. L,; Gigantic Enhancement in Sensitivity Using Schottky Contacted Nanowire Nanosensor, J. Am. Chem. Soc. 2009, 131, 17690-17695

[4] Yeh, P. H.; Li, Z.; Wang, Z. L,; Schottky-gated probe-free ZnO nanowire biosensor, Adv. Mater. 2009, 21, 4975-4978

[5] Zhou, J.; Gu, Y. D.; Hu, Y. F.; Mai, W. J.; Yeh, P. H.; Bao, G.; Sood, A. K.; Polla, D. L.; Wang, Z. L,; Appl. Phys. Lett. Gigantic enhancement in response and reset time of ZnO UV nanosensor by utilizing Schottky contact and surface functionalization, 2009, 94, 191103

[6] Weiwei, W.; Bai, S,; Cui, N,; Ma, F,; Wie, Z,; Qin, Y,; Xie, E,; Increasing UV Photon Response of ZnO Sensor with Nanowires Array, Sci. Adv. Mater. 2010, 94, 3, 402-406

[7] Eisner, C,; Cavakacbti, E,; Ferraz, O,; Sarli, A.R.; Evaluation of the surface treatment effect on the anticorrosive performance of paint systems on steel, Progress in Organic Coatings, 2003, 48, 50-62

[8] Wang, Z. L,; Mater. Today, The new field of nanopiezotronics, 2007, 10, 20-28

[9] Wang, Z. L,; Adv. Mater. Nanopiezotronics, 2007, 19, 889-892

[10] Wang, Z. L,; Towards self-powered nanosystems: From nanogenerators to nanopiezotronics, Adv. Funct. Mater. 2008, 18, 3553-3567

[11] King, P.D.C,; Veal, T.D,; Conductivity in transparent oxide semiconductors, J. Phys.: Condens. Matter, 2011, 23, 334214

[12] Wang, Z. L.; Song, J. H,; Piezoelectric nanogenerators based on zinc oxide nanowire arrays, Science 2006, 312, 242-246

[13] Wang, X. D.; Song, J. H.; Liu, J.; Wang, Z. L,; Direct-current nanogenerator driven by ultrasonic waves, Science, 2007, 316, 102-105

[14] Yang, R. S.; Qin, Y.; Dai, L. M.; Wang, Z. L,; Power generation with laterally packaged piezoelectric fine wires, Nat. Nanotechnol, 2009, 4, 34-39

[15] Law, M.; Greene, L. E.; Johnson, J. C.; Saykally, R.; Yang, P. D,; Nanowire dye-sensitized solar cells, Nat. Mater. 2005, 4, 455-459

[16] Levy-Clement, C.; Tena-Zaera, R.; Ryan, M. A.; Katty, A.; Hodes, G,; CdSe-sensitized p-CuSCN/nanowire n-ZnO heterojunctions, Adv. Mater. 2005, 17, 1512-1515

[17] Weintraub, B.; Wei, Y. G.; Wang, Z. L,; Optical fiber/ nanowire hybrid structures for efficient three-dimensional dye-sensitized solar cells, Angew. Chem. Int. Ed. 2009, 48, 8981-8985

[18] Wei, Y. G.; Xu, C.; Xu, S.; Li, C.; Wu, W. Z.; Wang, Z. L,; Planar waveguide-nanowire integrated three-dimensional dye- sensitized solar cells, Nano Lett. 2010, 10, 2092-2096

[19] Sun, K,; Madsen, K,; Andersen, P,; Bao, W,; Sun, Z,; and Wang, D,; Metal and metal oxide nanowire co-catalyzed Si photocathode, Nanotechnology, 2012, 23, 194013

[20] Sun, K,; Jing, Y,; Li, C,; Zhang, X,; Aguinaldo, R,; Kargar, A,; Madsen, K,; Banu, K,; Zhou, Y,; Bando, Y,; Liu, Z,; and Wang, D,; 3D branched nanowire heterojunction photoelectrodes for high-efficiency solar water splitting and H2 generation, Nanoscale, 2012, 4, 1515-1521

[21] Cui, J,; Zinc oxide nanowires, Materials Characterization, 2012, 64, 43-52

[22] Kumar, B.; Lee, K. Y.; Park, H. K.; Chae, S. J.; Lee, Y. H.; Kim, S. W,; Controlled growth of semiconducting nanowire, nanowall, and hybrid nanostructures on graphene for piezoelectric nanogenerators, ACS Nano, 2011, 5, 4197-4204

[23] Izaki, M.; Watanabe, M.; Aritomo, H.; Yamaguchi, I.; Asahina, S.; Shinagawa, T.; Chigane, M.; Inaba, M.; Tasaka, A,; Zinc oxide nano-cauliflower array with room temperature ultraviolet light emission, Cryst. Growth Des, 2008, 8, 1418-1421

[24] Zhang, H.; Yang, D.; Ji, Y. J.; Ma, X. Y; Xu, J.; Que, D. L,; Low temperature synthesis of flowerlike ZnO nanostructures by cetyltrimethylammonium bromide-assisted hydrothermal process, J. Phys. Chem. B 2004, 108, 3955-3958

[25] Wang, Z.; Qian, X. F.; Yin, J.; Zhu, Z. K,; Large-scale fabrication of tower-like, flower-like, and tube-like ZnO arrays by a simple chemical solution route, Langmuir, 2004, 20, 3441-3448

[26] Kim, C,; Kim, J.K,; Jang, E,; Yi, G,; Kim, H.K,; Whispering-gallery-modelike-enhanced emission from ZnO nanodisk, Appl. Phys. Lett. 2006, 88, 093104

[27] Long, T,; Yin, S,; Takabatake, K,; Zhnag, P,; Sato, T,; Synthesis and Characterization of ZnO Nanorods and Nanodisks from Zinc Chloride Aqueous Solution, Nanoscale Res Lett. 2009, 4, 247-253

[28] Chang, Y,; Yang, W,; Chang, C,; Hsu, P,; Chen, L; Controlled Growth of ZnO Nanopagoda Arrays with Varied Lamination and Apex Angles, Crystal Growth & Design, 2009, 9, 7

[29] Narasimhan, K.L,; Pai, S.P,; Palkar, V.R,; Pinto, R,; High quality zinc oxide films by pulsed laser ablation, Thin Solid Films, 1997, 295, 104-106

[30] Sun, K,; Wei, W,; Ding, Y,; Jing, Y,; Wang, Z,; Wang, D,; Crystalline ZnO thin film by hydrothermal growth, Chem. Commun., 2011, 47, 7776-7778

[31] Kim, J.H,; Kim, E,; Andeen, D,; Thomson, D,; DenBaars, S.P,; Lange, F.; Growth of heteroepitaxial ZnO thin films on GaN-buffered Al_2O_3(0001) substrates by low- temperature hydrothermal synthesis at 90 °C, Adv. Funct. Mater. 2007, 17, 463

[32] Tay, C.B,; Chua, S.J,; Loh, K.P,; Stable p-type doping of ZnO film in aqueous solution at low temperatures, J. Phys. Chem. C, 2010, 114, 9981-9987

[33] Fang, X,; Li, J,; Zhao, D,; Shen, D,; Li, B,; Wang, X,; Phosphorus-Doped p-Type ZnO Nanorods and ZnO Nanorod p-n Homojunction LED Fabricated by Hydrothermal Method, J. Phys. Chem. C, 2009**,** 113, 21208

[34] Chu, S,; Lim, J.H,; Mandalapu, L.J,; Yang, Z,; Li, L,; Liu, J.L,;
Sb-doped *p*-ZnO/Ga-doped *n*-ZnO homojunction ultraviolet light emitting diodes, App. Phys. Lett. 2008, 92, 152103

[35] Heo, Y. W.; Varadarajan, V.; Kaufman, M.; Kim, K.; Norton, D. P.; Ren, F.; Fleming, P. H,; Site-specific growth of ZnO nanorods using catalysis-driven molecular-beam epitaxy, Appl. Phys. Lett. 2002, 81, 3046-3048

[36] Chiou, W. T.; Wu, W. Y.; Ting, J. M,; Growth of single crystal ZnO nanowires using sputter deposition, Diam. Relat. Mater. 2003, 12, 1841-1844

[37] Sun, Y.; Fuge, G. M.; Ashfold, M. N. R,; ZnO nanorod arrays by catalyst-free pulsed laser deposition methods, Chem. Phys. Lett. 2004, 396, 21

[38] Hong, J. I.; Bae, J.; Wang, Z. L.; Snyder, R. L,; Room- temperature, texture-controlled growth of ZnO thin films and their application for growing aligned ZnO nanowire arrays, Nanotechnology 2009, 20, 085609

[39] Park, W. I.; Yi, G. C.; Kim, M. Y.; Pennycook, S. J,; Nanoneedles grown vertically on Si substrates by non-catalytic vapor-phase epitaxy, Adv. Mater. 2002, 14, 1841-1843

[40] Park, W. I.; Kim, D. H.; Jung, S. W.; Yi, G. C,; Metalorganic vapor-phase epitaxial growth of vertically well-aligned ZnO nanorods, Appl. Phys. Lett. 2002, 80, 4232-4234

[41] Yuan, H.; Zhang, Y,; Preparation of well-aligned ZnO whiskers on glass substrate by atmospheric MOCVD, J. Cryst. Growth 2004, 263, 119-124

[42] Laudise, R. A.; Ballman, A. A,; Hydrothermal synthesis of zinc oxide and zinc sulfide, J. Phys. Chem. 1960, 64, 688-691

[43] Verges, M. A.; Mifsud, A.; Serna, C. J,; Formation of rod- like zinc-oxide microcrystals in homogeneous solutions, J. Chem. Soc., Faraday Trans. 1990, 86, 959-963

[44] Vayssieres, L.; Keis, K.; Lindquist, S. E.; Hagfeldt, A,; Purpose-built anisotropic metal oxide material: 3D highly oriented microrod array of ZnO, J. Phys. Chem. B 2001, 105, 3350-3352

[45] Bobade, S.M,; A reconstruction of cubic rs-ZnO on MgO (200) substrate through (100) plane of w-ZnO:rs-ZnO for transparent electronic application, Appl. Phys. Lett. 2012, 100, 072102

[46] Baruah, S,; Dutta, J,; Hydrothermal growth of ZnO nanostructures, Sci. Technol. Adv. Mater. 2009, 10, 013001

[47] Wang, Z.L.; Zinc oxide nanostructures: growth, properties and applications, J. Phys.: Condens. Matter, 2004, 16, R829-R858

[48] Xu, S,; Wang, L,; One-Dimensional ZnO Nanostructures: Solution Growth and Functional Properties, Nano Res, 2011, 4, 11, 1013

[49] Demianets, L.N,; Kostomarov, D.V,; Mechanism of zinc oxide single crystal growth under hydrothermal conditions, Ann. Chim. ScL Mat, 2001, 26, 193-198

[50] Valtiner, M,; Borodin, S,; Grundmeier, G,; Stabilization and Acidic Dissolution Mechanism of Single-Crystalline ZnO(0001) Surfaces in Electrolytes Studied by In-Situ AFM Imaging and Ex-Situ LEED, Langmuir, 2008, 24, 5350-5358

[51] Yamabi, S.; Imai, H,; H. Growth conditions for wurtzite zinc oxide films in aqueous solutions, J. Mater. Chem. 2002, 12, 3773-3778

[52] Chemspider. 15, May, 2012 <www.chemspider.com/Chemical-Structure.3959.html>

[53] J. G. Strom, Jr. and H. W. Jun, Kinetics of hydrolysis of methenamine, J. Pharm. Sci., 1980, 69, 1261-1263

[54] Wang, H,; Xie, J,; Yan, K,; Duan, M,; H. Wang,; Growth Mechanism of Different Morphologies of ZnO Crystals Prepared by Hydrothermal Method, J. Mater. Sci. Technol. 2011, 27, 2, 153-158

[55] Sugunan A, Warad H C, Boman M and Dutta J,; Zinc oxide nanowires in chemical bath on seeded substrates: Role of hexamine, J. Sol–Gel Sci. Technol. 2006, 39**,** 49-56

[56] Gao, Y. F.; Nagai, M.; Chang, T. C.; Shyue, J. J,; Solution- derived ZnO nanowire array film as photoelectrode in dye- sensitized solar cells, Cryst. Growth Des. 2007, 7, 2467-2471

[57] Zhou, Z. Z.; Deng, Y. L,; Kinetics study of ZnO nanorod growth in solution, J. Phys. Chem. C, 2009, 113, 19853-19858

[58] Masel, R., 2001, Chemical Kinetics and Catalysis, John Wiley & Sons

[59] Tak, Y.; Yong, K. J,; Controlled growth of well-aligned ZnO nanorod array using a novel solution method, J. Phys. Chem. B, 2005, 109, 19263-19269

[60] Xu, S.; Wei, Y. G.; Liu, J.; Yang, R.; Wang, Z. L,; Integrated multilayer nanogenerator fabricated using paired nanotip-to-nanowire brushes, Nano Lett. 2008, 8, 4027-4032

[61] Sun, H. K.; Luo, M.; Weng, W. J.; Cheng, K.; Du, P.; Shen, G.; Han, G. R,; Position and density control in hydrothermal growth of ZnO nanorod arrays through pre-formed micro/ nanodots, Nanotechnology, 2008, 19, 395602

[62] Ma, T.; Guo, M.; Zhang, M.; Zhang, Y. J.; Wang, X. D,; Density-controlled hydrothermal growth of well-aligned ZnO nanorod arrays, Nanotechnology, 2007, 18, 035605

[63] Hsiao, C,; Pen, C,; Chen, S,; Tunable growth of ZnO nanorods synthesized in aqueous solutions at low temperatures, J. Vac. Sci. Technol. B, 2006, 24, 288-291

[64] Liou, S,; Hsiao, C,; Chen, S,; Growth behavior and microstructure evolution of ZnO nanorods grown on Si in aqueous solution, Journal of Crystal Growth, 2005, 274, 438-446

[65] Xu, S,; Lao, C,; Weintraub, B,; Wang, Z,; Density-controlled growth of aligned ZnO nanowire arrays by seedless chemical approach on smooth surfaces, J. Mater. Res. 2008, 23, 2072–2077

[66] Wu, W,; Hu G,; Cui, S,; Zhou, y,; Wu, H,; Epitaxy of vertical ZnO nanorod arrays on highly (001)- oriented ZnO seed monolayer by a hydrothermal route, Crys. Growth Des. 2008, 8, 11, 4014-4020

[67] Andeen, D.; Kim, J. H.; Lange, F. F.; Goh, G. K. L.; Tripathy, S. Lateral epitaxial overgrowth of ZnO in water at 90 °C, AdV. Funct. Mater. 2006, 16, 799-804

[68] Kosmulski, M.; "Chemical properties of materials surfaces." Dekker, New York, 2001

[70] Nicholas, N.J,; Franks, G,; Ducker, W,; Selective Adsorption to Particular Crystal Faces of ZnO, Langmuir, 2012, 28, 18, 7189-7197

[71] Joo, J,; Chow, B,; Prakash, M,; Boyden, E,; Jacobson, J,; Face-selective electrostatic control of hydrothermal zinc oxide nanowire synthesis, Nat. Mat. 2011, 10, 596

[72] Xi, Y.; Hu, C. G.; Han, X. Y.; Xiong, Y. F.; Gao, P. X.; Liu, G. B,; Solid State Commun. 2007, 141, 506-512

[70] Yang, J. H.; Liu, G. M.; Lu, J.; Qiu, Y. F.; Yang, S. H,; Electrochemical route to the synthesis of ultrathin ZnO nanorod/nanobelt arrays on zinc substrate, Appl. Phys. Lett. 2007, 90, 103109

[73] Jiang, H.; Hu, J.; Gu, F.; Li, C,; Self-assembly of solid or tubular ZnO rods into twinning microprisms via a hydrothermal route, J. Alloys Compd. 2009, 478, 550-553

[74] Vayssieres, L.; Keis, K.; Hagfeldt, A.; Lindquist, S. E,; Three-dimensional array of highly oriented crystalline ZnO microtubes, Chem. Mater. 2001, 13, 4395-4398

[75] Zhang, J.; Sun, L. D.; Liao, C. S.; Yan, C. H,; A simple route towards tubular ZnO, Chem. Commun. 2002, 262-263

[76] She, G. W.; Zhang, X. H.; Shi, W. S.; Fan, X.; Chang, J. C,; Electrochemical/chemical synthesis of highly-oriented single- crystal ZnO nanotube arrays on transparent conductive substrates, Electrochem. Commun. 2007, 9, 2784-2788

[77] Li, F.; Ding, Y.; Gao, P. X. X.; Xin, X. Q.; Wang, Z. L,; Single-cystal hexagonal disks and rings of ZnO: Low- temperature, large-scale synthesis and growth mechanism, Angew. Chem. Int. Ed. 2004, 43, 5238-5242

[78] Tian, Z. R. R.; Voigt, J. A.; Liu, J.; McKenzie, B.; McDermott, M. J.; Rodriguez, M. A.; Konishi, H.; Xu, H. F,; Complex and oriented ZnO nanostructures, Nat. Mater. 2003, 2, 821-826

[79] Zhang, T. R.; Dong, W. J.; Keeter-Brewer, M.; Konar, S.; Njabon, R. N.; Tian, Z. R,; Site-specific nucleation and growth kinetics in hierarchical nanosyntheses of branched ZnO crystallites, J. Am. Chem. Soc. 2006, 128, 10960-10968

[80] Liu, B,; Zeng, H.C,; Hydrothermal synthesis of ZnO nanorods in the diameter regime of 50 nm, J. Am. Chem. Soc. 2003**,** 125, 4430-4431

[81] Yuhas, B. D.; Zitoun, D. O.; Pauzauskie, P. J.; Yang, P,; Transition-metal doped zinc oxide nanowires, Angew. Chem. Int. Ed. 2006, 45, 420-423

[82] Han, T,; Meng, F.Y,; Zhang, S,; Cheng, X.M,; Oh, J.I,; Band gap and electronic properties of wurtzite-structure ZnO co-doped with IIA and IIIA, J. App. Phys. 2011, 110, 063724

[83] Fan, J,; Shavel, A,; Zamani, R,; Fabrega, C,; Rousset, J,; Haller, S,; Guell, F,; Carrete, A,; Andreu, T,; Arbiol, J,; M, J.R,; Cabot, A,; Control of the doping concentration, morphology and optoelectronic properties of vertically aligned chlorine-doped ZnO nanowires, Acta Materialia, 2011, 59, 6790-6800

[84] Chiu, S,; Lin, Y,; Lin, J,; Four-probe electrical-transport measurements on single indium tin oxide nanowires between 1.5 and 300 K, Nanotechnology, 2009, 20**,** 015203

[85] Look, D.C,; Hemsky, J.W,; Sizelove, J.R,; Residual Native Shallow Donor in ZnO**,** Phys. Rev. Lett. 1999, 82, 2552–2555

[86] Janotti, A,; Van de Walle, C,; Oxygen vacancies in ZnO, App. Phys. Lett. 2005, 87, 122102

[87] Van de Walle, C,; Defect analysis and engineering in ZnO, Physica B, 2001 308, 899-903

[88] Weber, J,; Hydrogen in semiconductors: From basic physics to technology (pages 535–538), phys. stat. sol. (c), 2008 5, 2, 535-538

[89] Nadarajah, A.; Word, R. C.; Meiss, J.; Konenkamp, R,; Flexible inorganic nanowire light-emitting diode, Nano Lett. 2008, 8, 534-537

[90] Pradhan, B,; Batabyal, S.K,; Pal, A.J,; Rectifying junction in a single ZnO vertical nanowire, Appl. Phys. Lett. 2006, 89, 233109

[91] Liu, W,; Xiu, F,; Sun, K,; Xie, Y.H,; Wang, K.L,; Wang, Y,; Zou, J,; Yang, Z,; Liu, J,; Na-Doped p-Type ZnO Microwires**,** J. Am. Chem. Soc. 2010, 132, 2498-2499

[92] He, H,; Lin, S,; Yuan, G,; Zhang, L,; Zhang, W.F,; Luo, L,; Cao, Y.L,; Ye, Z,; Lee, S.T.,; Single-Crystalline Sodium-Doped p-Type ZnO and ZnMgO Nanowires via Combination of Thin-Film and Nano Techniques, J. Phys. Chem. C, 2011, 115, 19018-19022

[93] Gupta, M.K,; Sinha, N,; Kumar, B,; J. p-type K-doped ZnO nanorods for optoelectronic applications, Appl. Phys. 2011, 109, 083532

[94] Yuan, G.D,; Zhang, W.J,; Jie, J.S,; Fan, X,; Zapien, J.A,; Leung, Y.H,; Luo, L.B,; Wang, P.F,; Lee, C.F,; Lee, S.T,; p-type ZnO nanowire arrays, Nano Lett. 2008, 8, 2591-2597

[95] Thomas, M,; Cui, J.B,; Electrochemical Route to p-Type Doping of ZnO Nanowires**,** J. Phys. Chem. Lett. 2010, 1, 1090-1094

[96] Xiang, B,; Wang, P,; Zhang, X,; Dayeh, S.A,; Aplin, D.P.R,; Soci, C,; Yu, D,; Wang, D,; Rational synthesis of p-type zinc oxide nanowire arrays using simple chemical vapor deposition, Nano Lett. 2007, 7, 323-328

[97] Cao, B,; Lorenz, M,; Rahm, A,; Von Wenckstern, H,; Czekalla, C,; Lenzner, J,; Benndorf, G,; Grundmann, M,; Phosphorus acceptor doped ZnO nanowires prepared by pulsed-laser deposition, Nanotechnology, 2007, 18, 455707

[98] Yu, D,; Li, J,; Hu, L,; Hu, H,; Zhang, H,; Sun, K,; Zhu, J,; Synthesis and photoluminescence investigation of ZnO : P nanorods on an InP substrate by pulsed laser deposition, Chem. Phys. Lett. 2008, 464, 69-72

[99] Fang, X,; Li, J,; Zhao, D,; Shen, D,; Li, B,; Wang, X,; Phosphorus-Doped p-Type ZnO Nanorods and ZnO Nanorod p-n Homojunction LED Fabricated by Hydrothermal Method, J. Phys. Chem. C, 2009, 113, 21208-21212

[100] Zhang, J.Y,; Li, P.J,; Sun, H,; Shen, X,; Deng, T.S,; Zhu, K.T,; Zhang, Q.F,; Wu, J.L,; Ultraviolet electroluminescence from controlled arsenic-doped ZnO nanowire homojunctions, Appl. Phys. Lett. 2008, 93, 021116

[101] Sun, M,; Zhang, Q.F,; Wu, J.L,; Electrical and electroluminescence properties of As-doped p-type ZnO nanorod arrays, J. Phys. D: Appl. Phys. 2007, 40, 3798-3802

[102] Wang, F,; Seo, J.H,; Bayerl, D,; Shi, J,; Mi, H,; Ma, Z,; Zhao, D,; Shuai, Y,; Zhou, W,; Wang, X,; An aqueous solution-based doping strategy for large-scale synthesis of Sb-doped ZnO nanowires, Nanotechnology, 2011, 22, 225602

[103] Chu, S,; Wang, G,; Zhou, W,; Lin, Y,; Chernyak, L,; Zhao, J,; Kong, J,; Li, L,; Ren, J,; Liu, J,; Electrically pumped waveguide lasing from ZnO nanowires, Nat. Nanotechnology, 2011, 6, 506

[104] Briscoe, J,; Gallardo, D.E,; Dunn, S,; In situ antimony doping of solution-grown ZnO nanorods, Chem. Commun., 2009, 1273-1275

[105] Limpijumnong, S,; Zhang, S.B,; Wei, S,; Park, C.H,; Doping by Large-Size-Mismatched Impurities: The Microscopic Origin of Arsenic- or Antimony-Doped p-Type Zinc Oxide, Phys. Rev. Lett. 2004, 92, 15, 155504

[106] Wahl, U,; Correia, J.G,; Mendonca, T,; Decoster, S,; Direct evidence for Sb as a Zn site impurity in ZnO, App. Phys. Lett. 2009, 94, 261901

[107] Lange's Handbook of Chemistry, 10th ed. McGraw-Hill, 1973 pp1496-1505

[108] Chemspider. 15, May, 2012 <www.chemspider.com/Chemical-Structure.6146.html>

[109] Li, F,; Ding, Y,; Gao, P,; Xin, X,; Wang, Z.L,; Single-Crystal Hexagonal Disks and Rings of ZnO: Low-Temperature, Large-Scale Synthesis and Growth Mechanism, Angew. Chem. 2004, 116, 5350-5354

[110] Gao, P,; Ying, C,; Wang, S,; Ye, L,; Guo, Q,; Xie, Y,; Low temperature hydrothermal synthesis of ZnO nanodisk arrays utilizing self-assembly of surfactant molecules at solid–liquid interfaces, Journal of Nanoparticle Research, 2006, 8, 131-136

[111] Cao, H.L,; Qian, X.F,; Gong, Q,; Du, W.M,; Ma, X.D,; Zhu, Z.K,; Shape- and size-controlled synthesis of nanometre ZnO from a simple solution route at room temperature, Nanotechnology, 2006, 17, 3632-3636

[112] Kuppusami, P,; Vollweiler, G,; Rafaja, D,; Ellmer, K,; Epitaxial growth of aluminium-doped zinc oxide films by magnetron sputtering on (001), (110), and (012) oriented sapphire substrates, Appl. Phys. A, 2005, 80, 183-186

[113] Phan, D,; Chung, G,; Characteristics of ZnO Films Deposited on Poly 3C-SiC Buffer Layer by Sol-Gel Method transactions on electrical and electronic materials, 2011, 12, 3, 102-105

[114] Myung, J.H,; Kim, N.H,; Kim, H,W,; Structural Properties of Sputter-Deposited ZnO Thin Films Depending on the Substrate Materials, Materials Science Forum, 2005, 475, 1825-1828

[115] Izquierdo, R,; Sacher, E,; Yelon, A,; X-ray photoelectron spectra of antimony oxides, Applied Surface Science, 1989, 40, 175-177

[116] Lupan, O,; Chow, L,; Ono, L,; Cuenya, B.R,; Chai, G,; Khallaf, H,; Park, S,; Schulte, A,; Synthesis and Characterization of Ag- or Sb-Doped ZnO Nanorods by a Facile Hydrothermal Route, J. Phys. Chem. C, 2010, 114, 12401-12408

[117] Nicholas, N.J,; Franks, G.V,; Ducker, W.A,; The mechanism for hydrothermal growth of zinc oxide, CrystEngComm, 2012, 14, 1232-1240

[118] Ip, K,; Overberg, M.E,; Heo, Y.W,; Norton, D.P,; Pearton, S.J,; Kucheyev, S.O,; Jagadish, C,; Williams, J.S,; Wilson, R.G,; Zavada, J.M,; Thermal stability of ion-implanted hydrogen in ZnO, App. Phys. Lett. 2002, 81, 2, 3996-3998